nature communications

Article

https://doi.org/10.1038/s41467-025-65446-z

Complementarity fusion of boron-oxygen and carbazole blocks enables narrowband blue OLEDs with high performance

Received: 14 June 2025

Accepted: 15 October 2025

Published online: 25 November 2025

Check for updates

Guo Yuan[1,4], Yan-Chun Wang[1,4], Zhen Zhang[2] ✉, Jun-Yu Liu[1], Yi-Hui He[2], Guo-Wei Chen[3], Yan-Qing Li[2] ✉ & Jian-Xin Tang[1,3] ✉

The development of ultra-high-definition organic light-emitting diodes (OLEDs) displays requires efficient and narrowband blue emission. Nevertheless, binary host-guest doped narrowband blue OLEDs still face significant challenges in simultaneously realizing high efficiency and negligible roll-off. Herein, a molecular construction strategy through the synergistic interplay between π-conjugation extension and functional complementarity fusion is proposed by incorporating a rigid boron-oxygen (BO) framework with carbazole building blocks. The constructed compounds exhibit increased triplet exciton recycling capability, high excited-state energy levels, and improved charge transporting features, showcasing significant potential as host matrices for blue devices. The sensitizer-free OLEDs achieve the narrowband blue emission with a CIEy value lower than 0.15, a maximum external quantum efficiency of 41.2%, and the suppressed efficiency roll-off at high luminance due to efficient energy transfer to blue guest emitters and elevated horizontal dipole orientation. This work strategically demonstrates a balance between high efficiency and reduced efficiency roll-off in binary narrowband blue OLEDs, representing a substantial advancement in blue electroluminescent technology.

With the rapidly growing demand for ultra-high-definition (UHD) displays in modern electronics, the evolution of organic light-emitting diodes (OLEDs) displaying both high efficiency and narrowband emission has witnessed flourishing progress[1–3]. As a critical metric for color purity, spectral narrowing engineering of organic emitters has emerged as a pivotal research direction[4–6]. Distinct from conventional approaches utilizing optical filters or microcavity structures for spectral modulation, thermally activated delayed fluorescence (TADF) compounds with multiresonance (MR) topology enable fairly sharp single-peaked narrowband emission, offering substantial prospects for UHD display applications[7–10]. Nevertheless, constrained by the slow reverse intersystem crossing (RISC) process, long-lived triplet excitons in blue MR emitters undergo high-density accumulation during device operation, inducing detrimental bimolecular quenching phenomena known as triplet-triplet annihilation (TTA) and triplet-polaron annihilation (TPA)[11,12]. Therefore, the corresponding devices typically exhibit severe efficiency roll-off under high luminance conditions, posing significant challenges to further development of narrowband blue OLEDs[13,14]. An effective mitigation strategy involves implementing the hyperfluorescence (HF) technology through ternary sensitized HF systems (host + TADF/phosphorescent sensitizer + MR-TADF emitter), where TADF or phosphorescent molecules serve as exciton harvesters to collect and recycle triplet excitons[15–17]. Subsequent energy transfer processes enable efficient energy migration to terminal MR

[1]Jiangsu Key Laboratory for Carbon-Based Functional Materials & Devices, Institute of Functional Nano & Soft Materials (FUNSOM), Soochow University, Suzhou, China. [2]School of Physics and Electronic Science, East China Normal University, Shanghai, China. [3]Macao Institute of Materials Science and Engineering (MIMSE), Faculty of Innovation Engineering (FIE), Macau University of Science and Technology, Taipa, China. [4]These authors contributed equally: Guo Yuan, Yan-Chun Wang. ✉e-mail: zzhang@phy.ecnu.edu.cn; yqli@phy.ecnu.edu.cn; jxtang@must.edu.mo

emitters[18,19]. However, the HF technology also introduces problems, including intricate ternary co-evaporation processes for emissive layer fabrication and potential material degradation in multiple-component emitting systems. These inherent complexities impose stringent requirements on both the development of advanced organic luminescent materials and the optimization of OLED device architectures[20,21].

In narrowband blue OLEDs, to simultaneously meet the requirements of high efficiency and low roll-off without increasing device fabrication complexity, the host materials based on a boron-oxygen (BO) framework have recently indicated significant potential in binary host-guest doping systems for blue OLEDs[22,23]. In 2019, Hatakeyama et al. demonstrated a BO-modified host molecule (DOBNA-OAr) for the blue *ν*-DABNA emitter, achieving a maximum external quantum efficiency (EQE_{max}) of 34.4%, while maintaining an EQE of 26.0% at a high brightness of 1000 cd m^{-2} (EQE_{1000})[24]. Furthermore, in 2021, utilizing a BO-bridged host named DOBNA-Tol, they achieved an EQE_{max} of 29.5% in combination with the blue emitter *ν*-DABNA-O-Me, exhibiting minimal efficiency roll-off (EQE_{1000} = 26.9%)[25]. However, the relatively deep LUMO energy level results in an energy mismatch with blue MR-TADF emitters. To further enhance the electroluminescent (EL) performance of narrowband blue OLEDs through host engineering optimization, Park et al. developed a variety of MR-TADF hosts derived from an optimized BO-containing molecule, TDBA[26]. Through covalently integrating tetraphenylsilane (TPS) with the TDBA, the weak charge transfer (CT) effect between these units preserves the intrinsic MR-TADF characteristics of the TDBA core. Simultaneously, the TPS moiety enhances intermolecular spacing, effectively suppressing triplet exciton (T_1) quenching. Ultimately, leveraging the advantageous TADF properties and efficient Förster resonance energy transfer (FRET), the TDBA-Si: *ν*-DABNA-based device achieves an EQE_{max} of 36.2%.

Although BO-embedded hosts have demonstrated notable progress in enhancing the performance of blue OLEDs, the intrinsically limited frontier molecular orbital (FMO) distribution of BO frameworks often results in substantial overlap between the highest occupied molecular orbital (HOMO) and lowest unoccupied molecular orbital (LUMO) distributions, leading to relatively large singlet-triplet energy difference (ΔE_{ST}) and consequently restricted reverse intersystem crossing rate (k_{RISC})[22,27]. For binary-doped host-guest emissive systems, rapid triplet exciton recycling through TADF hosts is critically essential for improving device efficiency while maintaining high EQE at elevated brightness levels. A strategic approach involves π-conjugation extension of BO frameworks to modulate FMO distribution, thereby reducing ΔE_{ST} and accelerating the RISC process—a methodology extensively employed in constructing MR-TADF guest emitters[28]. Concurrently, considering the prerequisite of high T_1 energy levels in host materials for blue emitters to facilitate unidirectional energy transfer, a viable approach incorporates wide excited energy gap moieties such as carbazole (Cz) units into the molecular architecture[29]. Owing to its high T_1 and favorable hole-transport properties, the Cz block serves as an optimal candidate for constructing hole-transport-dominant host materials[30].

Recently, Tae Geun Kim's research team engineered an adamantane-incorporated host, Ad-mCP, by integrating adamantane substituents into mCP[31]. The rigid adamantane units enhanced morphological stability and thermal resistance, enabling blue narrowband OLEDs with Ad-mCP to achieve an EQE_{max} of 29.9%. In addition, Duan et al. developed an asymmetric deep-blue MR-TADF emitter, A-BN, which attained an EQE_{max} of over 40% when doped into the mCBP host[32]. However, the implementation of such unipolar transport materials induces interface-biased exciton recombination and a drastic surge in exciton concentration, fundamentally constraining the high-efficiency performance of devices at elevated current densities[33]. This necessitates the exploration of advanced host design strategies to further optimize exciton utilization and energy transfer. As aforementioned, the incorporation of Cz moieties into BO frameworks is anticipated to achieve more delocalized FMO distributions[34], thereby accelerating the recycling process of triplet excitons. Synergistically leveraging carbazole's high excited-state energy levels and favorable hole-transport capabilities, this molecular engineering approach enables the development of promising host materials with enhanced operational stability and energy transfer efficiency, which would simultaneously enhance the efficiency of blue OLEDs and effectively mitigate efficiency roll-off[31,35]. However, studies examining this strategy remain underexplored in the current literature.

Here, we propose a functionally complementary fusion strategy that integrates a rigid BO-bridged framework with electron-transporting characteristics and hole-transporting Cz moieties possessing high triplet energy levels (Fig. 1). In contrast to the aforementioned state-of-the-art BO-based host materials (e.g., DOBNA-Tol, TDBA-Si), we achieved the π-conjugation extension through intramolecular cyclization engineering that fuses the BO framework with carbazole units. The resulting fused architecture, denoted as BOCz, effectively prolongs FMO delocalization through π-conjugation extension of Cz moieties, thereby inducing moderate CT characteristics[36]. This structural modification is anticipated to reduce ΔE_{ST} while accelerating the RISC process. Guided by this strategic paradigm, two TADF materials, BOCzSi and 2BOCzSi, have been rationally designed. Through synergistic integration of π-conjugation extension and a functional complementarity fusion strategy between BO and Cz units, both compounds demonstrate elevated excited-state energy levels, favorable TADF characteristics, and accelerated RISC rates, showcasing significant potential as high-performance host candidates for blue OLEDs. Molecular structure-property optimization further elucidates the critical influence of exciton recycling kinetics, energy transfer, and charge transport properties on the operational efficacy of blue devices. To deeply validate their advantage as blue MR-TADF hosts, OLEDs were fabricated using the representative narrowband emitter, *ν*-DABNA, as the terminal guest. Owing to good exciton recycling capability and more efficient energy transfer processes, the BOCzSi-based sensitizer-free blue OLEDs demonstrated a remarkably high efficiency, with an EQE_{max} exceeding 40% (41.2%) alongside improved resistance to efficiency roll-off at higher luminance (1000 cd m^{-2}), simultaneously sustaining an EQE above 30% (31.6%), while also exhibiting blue electroluminescence at 468 nm accompanied by a spectral full width at half maximum (FWHM) of 18 nm. This study presents an effective strategy of functionally complementary fusion to facilitate the realization of the high-performance potential of blue MR-TADF materials. It also elucidates the molecular design-performance correlations of these organic functional materials, paving the way for the advancement of highly efficient narrowband blue OLEDs.

Results

Molecular construction and analysis

As illustrated in Fig. 1, our molecular design strategy reveals the construction of the material core (BOCz) through functionally complementary fusion of BO and Cz units. The strategic incorporation of Cz units enables effective π-conjugation extension within the molecular framework, thereby enhancing the TADF characteristics. Concurrently, carbazole's effective hole-transport capabilities significantly improve the charge transport properties of the material system, thus enabling the fabrication of hosts with improved charge transport capabilities. The introduction of bulky tert-butyl and tetraphenylsilane groups suppresses stacking of planarized MR-TADF emitters and mitigates exciton quenching[37]. This optimization is imperative for enhancing device efficiency. Furthermore, the asymmetric design paradigm enables systematic investigation into the correlation between precisely modulated exciton recycling kinetics, energy

https://doi.org/10.1038/s41467-025-65446-z

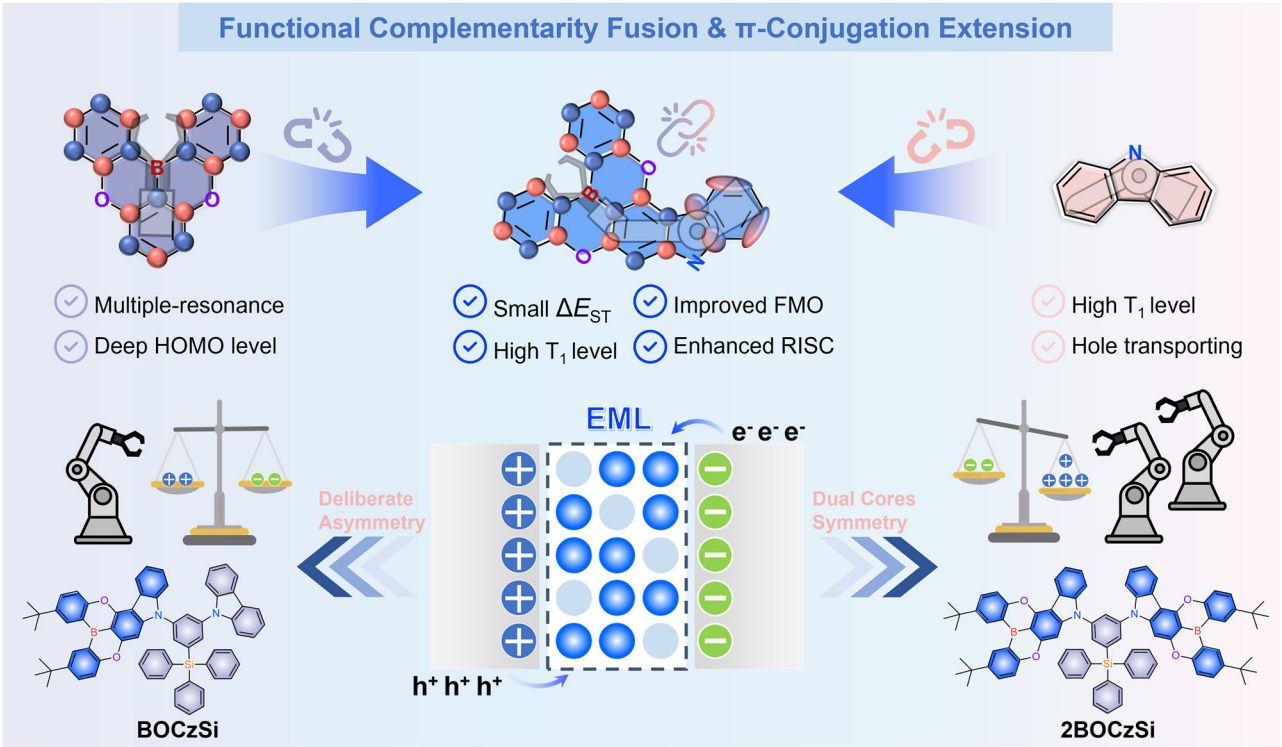

Fig. 1 | Schematic illustration of molecular design strategy. The multifunctional building block integrating boron-oxygen and carbazole modulates electronic delocalization, exciton dynamics, and charge transfer.

Table 1 | Photophysical properties of BOCzSi and 2BOCzSi

Compound	λ_{abs}[a] [nm]	λ_{PL}[a] [nm]	S_1[b] [eV]	T_1[b] [eV]	ΔE_{ST}[c] [eV]	PLQY[d] [%]	τ_p[e] [ns]	τ_d[e] [μs]	HOMO[f] [eV]	LUMO[g] [eV]	E_g[h] [eV]	T_d[i] [°C]
BOCzSi	302/346/382	425	3.13	2.95	0.18	40	11.5	0.45	−5.90	−2.99	2.91	454
2BOCzSi	305/348/380	425	3.16	2.93	0.23	38	11.9	1.30	−5.93	−2.99	2.94	506

[a]In toluene solution (1×10^{-5} m) at 298 K.
[b]Deduced from the fluorescence and phosphorescence spectra at 77 K.
[c]$\Delta E_{ST} = S_1 - T_1$.
[d]Measured in neat films.
[e]Prompt decay and delayed fluorescence lifetime in neat films.
[f]Obtained from ultraviolet photoelectron spectroscopy.
[g]Determined through summation of the optical band gaps with the corresponding HOMO energy levels.
[h]Obtained from the onset of the UV-vis absorption spectra.
[i]Decomposition temperatures measured by thermogravimetric analysis.

transfer efficiency, and charge transport properties in host materials with the performance metrics of blue OLED devices[38].

The synthetic routes and detailed procedures for the molecules, **BOCzSi** and **2BOCzSi**, can be found in the Supporting Information (Supplementary Fig. 1). The BOCz unit was synthesized through palladium-catalyzed Buchwald-Hartwig reaction-mediated intramolecular cyclization, followed by cross-coupling with commercially available dibromotetraphenylsilane to furnish the desired products. The obtained products were purified by column chromatography and vacuum sublimation for OLED device fabrication. The molecular architectures of intermediates and target compounds were unambiguously elucidated through nuclear magnetic resonance (NMR) and high-resolution mass spectrometry (Supplementary Figs. 2–10).

The electrochemical properties of the compounds were investigated using cyclic voltammetry (CV). The CV measurements revealed that both BOCzSi and 2BOCzSi exhibit reversible redox processes (Supplementary Fig. 11). The HOMO energy levels of the compound were estimated by ultraviolet photoelectron spectroscopy (UPS), with values of −5.90 eV for BOCzSi and −5.93 eV for 2BOCzSi (Supplementary Fig. 12 and Table 1). The decomposition temperature (T_d, equating to 5% weight loss) was established through thermogravimetric analysis (TGA) undertaken in a nitrogen atmosphere to examine the thermal stability of the materials. Supplementary Fig. 11 illustrates that BOCzSi and 2BOCzSi exhibited thermal decomposition temperatures of 454 and 506 °C, respectively, demonstrating good thermal stability that is advantageous for vacuum deposition processes in OLED device fabrication.

Theoretical calculations

To attain deeper insights into the geometric and electronic configurations of the two molecules, density functional theory (DFT) and time-dependent DFT (TD-DFT) theoretical simulations were conducted utilizing the Gaussian 16 software package at the B3LYP/6-31G(d) level[39]. As demonstrated in Fig. 2, the dihedral angles of BOCzSi and 2BOCzSi showed the values of 51.20°/50.25° for BOCzSi and 41.54°/57.58° for 2BOCzSi, respectively. The HOMO and LUMO of

https://doi.org/10.1038/s41467-025-65446-z

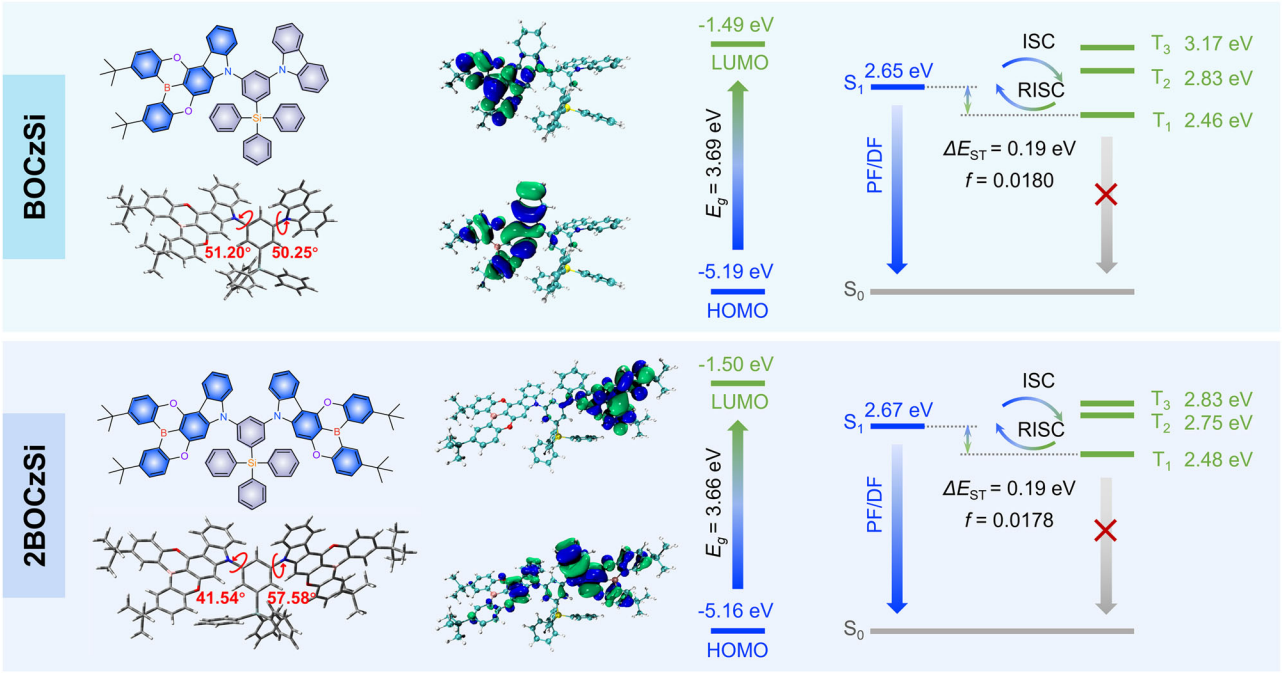

Fig. 2 | Density-functional theory calculation. Molecular structures, optimized geometries, FMO distributions, oscillator strengths, and excited energy state levels of BOCzSi and 2BOCzSi.

BOCzSi and 2BOCzSi are predominantly localized on the BOCz units. As anticipated, the π-conjugated fusion between BO and Cz moieties extends the FMO distribution toward the carbazole units, owing to their moderate CT characteristics. This constrained CT interaction simultaneously expands the spatial separation of HOMO and LUMO distributions while reducing their orbital overlap, thereby contributing to diminished ΔE_{ST} and optimized TADF characteristics. Furthermore, the FMOs do not exhibit significant extension toward the TPS groups. Therefore, the TPS groups are not likely to affect the electrochemical and photophysical properties of BOCzSi and 2BOCzSi. Interestingly, similar LUMO distributions are observed between BOCzSi and 2BOCzSi, whereas the distinct differences can be found in their HOMO distributions. For BOCzSi, both HOMO and LUMO are primarily distributed across the atoms comprising the entire BOCz framework. In contrast, the presence of an additional BOCz moiety in 2BOCzSi induces an extension of the HOMO toward this extra unit. This subtle modulation of the electronic structures will further influence the charge transfer characteristics and enable fine-tuning of the energy levels. The HOMO/LUMO energies were estimated to be −5.19/−1.49 eV for BOCzSi and −5.16/−1.50 eV for 2BOCzSi, respectively. Theoretical calculations reveal that the BOCz unit, formed through rational molecular design, retains the MR characteristics of the BO framework while optimizing FMO distributions. This structural refinement results in reduced ΔE_{ST} for both BOCzSi and 2BOCzSi, consequently enabling these compounds to exhibit favorable TADF features alongside efficient triplet exciton recycling processes (Supplementary Figs. 13, 14). To further clarify the influence of the BOCz fragment and molecular architecture on k_{RISC} of the emitters, the calculation of spin-orbit couplings (SOCs) was performed for both compounds (Supplementary Table 1). BOCzSi exhibited a SOC matrix element (SOCME) value of 0.1965 cm^{-1} between S_1 and T_1, nearly twice that of 2BOCzSi (0.1077 cm^{-1}). Therefore, BOCzSi evidences a more efficient RISC through the T_1 to S_1 channel. Besides, it is noteworthy that the higher-lying triplet states of BOCzSi exhibit a different natural transition orbital (NTO) distribution pattern as compared to 2BOCzSi, manifesting long-range CT or hybridized local and charge transfer (HLCT) characteristics. Consequently, BOCzSi demonstrates a larger SOCME than 2BOCzSi, contributing to a significant enhancement in its k_{RISC} value. Furthermore, theoretical calculations confirm that these compounds successfully retain the deep HOMO energy levels inherent to the BO unit while preserving the elevated T_1 of the carbazole moiety, thereby substantiating their potential as high-performance host materials.

Photophysical properties

Ultraviolet-visible (UV-vis) absorption and photoluminescence (PL) spectra of BOCzSi and 2BOCzSi in toluene solution were measured to investigate the photophysical features of these compounds. Figure 3 and Table 1 present the corresponding spectral profiles and parameters for each molecule. Both hosts exhibit nearly identical absorption behaviors, with peak wavelength (λ_{max}) observed at 300, 316, and 346 nm, likely attributed to diverse π−π* transitions of aryl moieties (including Cz functional groups) in toluene solution. The wide absorption band near 380 nm could be linked to n−π* transitions, potentially arising from electron transfer processes between carbazole-based units and BO moieties. Furthermore, the optical band gaps of BOCzSi and 2BOCzSi, calculated from the UV-vis absorption spectra of their neat films, were determined to be 2.91 and 2.94 eV, respectively. Based on these values and the HOMO levels obtained from UPS, the LUMO energy levels were calculated to be −2.99 eV for both BOCzSi and 2BOCzSi (Supplementary Fig. 15 and Table 1). Consequently, the incorporation of the BOCz moiety enables the effective modulation of energy levels, thereby improving the compatibility with blue MR-TADF emitters. PL spectra of BOCzSi and 2BOCzSi show maximum emission wavelengths recorded at 425 nm. The S_1/T_1 energy levels of both hosts were evaluated based on the fluorescence and phosphorescence (77 K) onset wavelengths. BOCzSi and 2BOCzSi exhibit S_1/T_1 energies of 3.13/2.95 eV and 3.16/2.93 eV, respectively. These results demonstrate sufficiently high T_1 values to enable efficient energy transfer to blue TADF emitters. Photophysical characterization reveals that BOCzSi and 2BOCzSi exhibit ΔE_{ST} values of 0.18 and 0.23 eV, respectively. Furthermore, a similarly small ΔE_{ST} can be observed in dilute toluene solutions (Supplementary Fig. 16). The reduced ΔE_{ST}, as theoretically predicted, arises from the delocalized

https://doi.org/10.1038/s41467-025-65446-z

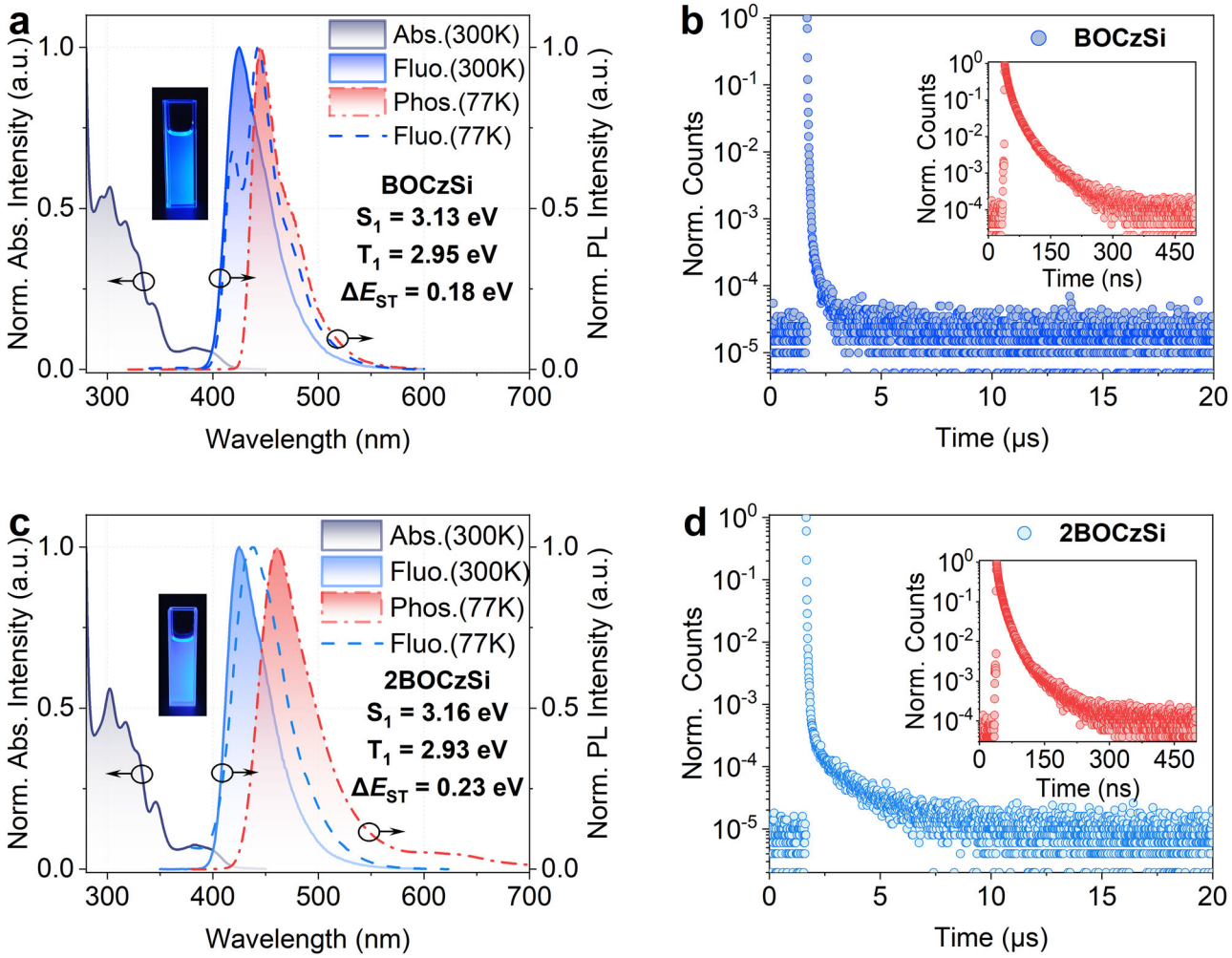

Fig. 3 | Photophysical property of BOCzSi and 2BOCzSi. UV-vis absorption, fluorescence (in toluene and neat films), and phosphorescence (in neat films) spectra of **a** BOCzSi and **c** 2BOCzSi. Transient photoluminescence decay spectra of **b** BOCzSi and **d** 2BOCzSi in neat films.

FMO distributions achieved through π-conjugation extension, indicating their promising potential for favorable TADF characteristics.

To evaluate the TADF features of BOCzSi and 2BOCzSi, transient photoluminescence (TRPL) decay profiles of their neat films were systematically investigated (Fig. 3b, d). Distinct delayed components were observed for both compounds, with corresponding delayed lifetimes of 0.45 and 1.30 μs, respectively. The delayed fluorescence lifetime is significantly shortened as compared to conventional BO-based host materials, attributable to the effective fusion of the BO framework with carbazole units through intramolecular cyclization engineering. Concurrently, these molecules exhibit pronounced temperature-dependent delayed emission, characteristic of TADF mechanisms (Supplementary Fig. 17 and Supplementary Table 2). From their TRPL decay profiles and photoluminescence quantum yields (PLQY) values of neat films, the k_{RISC} of BOCzSi and 2BOCzSi are calculated as 3.2×10^6 and $1.1 \times 10^6\,s^{-1}$, respectively. The k_{RISC} value exhibits an approximately one-order-of-magnitude enhancement as compared to that of the reported BO-type hosts, demonstrating the triplet exciton harvesting capability in BOCz-based host materials and validating the effectiveness of the multifunctional fusion-complementary strategy. Taking into account the intermolecular interactions arising from solid-state packing in pure thin films, TRPL measurements were conducted for both compounds in oxygen-free toluene solutions (Supplementary Fig. 18 and Supplementary Table 3). Similarly, the short delayed lifetimes of 0.43 and 0.86 μs were observed for BOCzSi and 2BOCzSi, respectively. It is noteworthy that in the solution state, we observed significantly higher PLQY for these two compounds compared to that in the film state, which is consistent with expectations. Although bulky tert-butyl and tetraphenylsilyl groups have been introduced, molecular packing in the neat film still leads to certain non-radiative processes. This observation aligns with the lower radiative decay rate (k_r) and higher non-radiative decay rate (k_{nr}) detected in the neat film state. Based on the PLQY values of BOCzSi and 2BOCzSi in toluene solution, their respective k_{RISC} values were calculated to be 2.8×10^6 and $1.5 \times 10^6\,s^{-1}$, which are consistent with the results obtained in the film state. These rapid RISC rates indicate that both BOCzSi and 2BOCzSi compounds possess inherent and efficient TADF characteristics. The shorter delayed lifetime observed in BOCzSi correlates with an enhanced RISC rate. This accelerated TADF-mediated spin-flip transition from triplet to singlet states effectively suppresses undesirable chemical degradation pathways associated with triplet excitons. Consequently, BOCzSi demonstrates enhanced triplet exciton recycling capability compared to 2BOCzSi. The collective results substantiate their pronounced potential as high-performance blue-emitting hosts.

Electroluminescent performance

Given the substantial potential of the materials, binary-doped OLED devices employing the synthesized BOCzSi and 2BOCzSi as hosts in the emissive layer were fabricated, while their EL performance was systematically researched. *ν*-DABNA was selected as the guest emitter for investigation because it is representative in terms of efficiency, color

https://doi.org/10.1038/s41467-025-65446-z

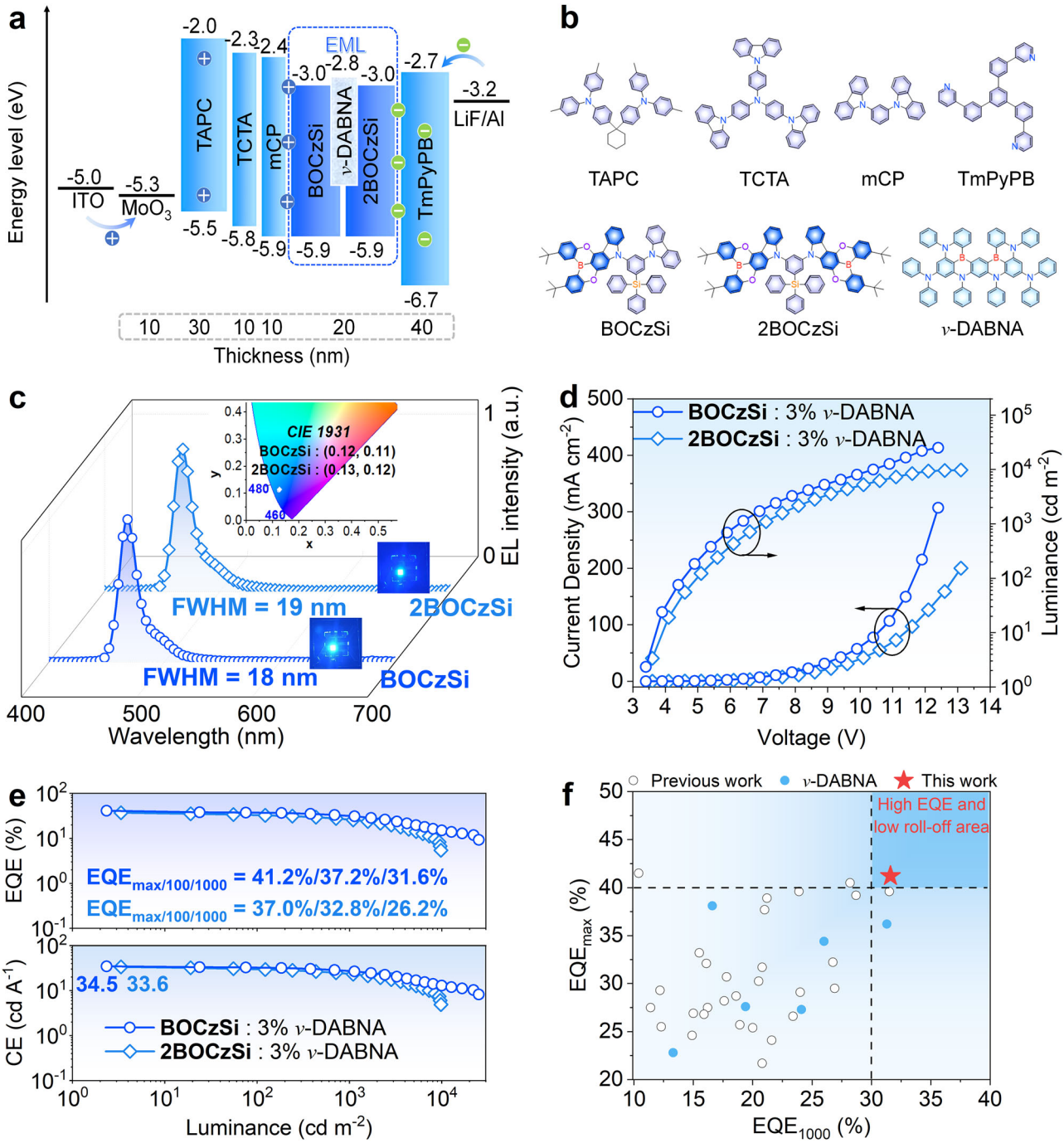

Fig. 4 | EL performance of binary non-sensitized OLEDs based on BOCzSi and 2BOCzSi host materials. a Device configuration and the energy level diagrams in BOCzSi/2BOCzSi-based OLEDs. **b** Chemical structures of employed materials. **c** EL spectra (inset: CIE chromaticity coordinates measured at a brightness of 100 cd m^{-2}). **d** Current density–voltage–luminance (*J*–*V*–*L*) curves. **e** EQE–L and CE–L curves. **f** Summary of representative deep-blue binary host-guest doping OLEDs (CIEy < 0.15).

purity, and emission wavelength. The T_1 energy level of *ν*-DABNA (2.62 eV) is lower than those of both BOCzSi and 2BOCzSi, ensuring the directional energy transfer. Furthermore, the HOMO level of *ν*-DABNA at −5.4 eV exhibits good matching with BOCzSi and 2BOCzSi, facilitating the efficient charge injection. Additionally, the host material employed in this work incorporates bulky tert-butyl and tetraphenylsilyl groups. This molecular design effectively disperses the *ν*-DABNA guest molecules, thereby suppressing the detrimental intermolecular interactions and enhancing the EL performance. The device architecture was ITO/molybdenum oxide (MoO_3, 10 nm)/1,1-bis[4-[*N*,*N*-di(p-tolyl)amino]phenyl]cyclohexane (TAPC, 30 nm)/4,4′,4″-Tris(carbazol-9-yl)triphenylamine (TCTA, 10 nm)/1,3-bis(*N*-carbazolyl) benzene (mCP, 10 nm)/hosts: 3% *ν*-DABNA (20 nm)/1,3,5-tris(3-pyridyl-3-phenyl)benzene (TmPyPB, 40 nm)/LiF(1 nm)/Al (100 nm).

Figure 4a and b schematically illustrate the device structure and molecular configurations, accompanied by their corresponding energy level alignments, and the data of other materials included in the device configuration were obtained in accordance with previously reported literature[10,18,24,31]. The EL spectra of both devices exhibit narrowband blue emission originating from *ν*-DABNA, with identical emission peaks centered at 468 nm (Fig. 4c and Table 2). Notably, the BOCzSi-containing device demonstrates a slightly narrower FWHM

Table 2 | EL performance of OLED devices based on BOCzSi and 2BOCzSi

EMLs	λ_{EL}/FWHM[a] [nm]	V_{on}[b] [V]	CE[c] [cd A^{-1}]	L_{max}[d] [cd m^{-2}]	EQE[e] [%]			CIE[f] [x, y]
					Max.	100 cd m^{-2}	1000 cd m^{-2}	
BOCzSi: 3 wt% *ν*-DABNA	468/18	3.4	34.5	25,170	41.2	37.2	31.6	(0.12, 0.11)
2BOCzSi: 3 wt% *ν*-DABNA	468/19	3.6	33.6	9802	37.0	32.8	26.2	(0.13, 0.12)

[a]The EL peak wavelength and full width at half maximum.
[b]Turn-on voltage at 1 cd m^{-2}.
[c]Maximum current efficiency.
[d]Maximum luminance.
[e]Maximum external quantum efficiency.
[f]Value taken at 100 cd m^{-2}.

(18 nm) compared to that of 2BOCzSi-employing OLED (19 nm), which could probably be attributed to more complete FRET between BOCzSi and the *ν*-DABNA emitter. The comparative analysis of EL characteristics among devices employing distinct host material systems demonstrates that the devices incorporating BOCzSi moieties exhibit enhanced EL performance. The maximum current efficiencies (CEs) of the devices manufactured utilizing BOCzSi, or 2BOCzSi as the hosts, were 34.5 and 33.6 cd A^{-1}, respectively. The EQE_{max} values were 41.2% and 37.0%, respectively. Moreover, the device employing BOCzSi as the host demonstrated a high EQE of 31.6% even at a high brightness of 1000 cd m^{-2}. This work has successfully achieved an EQE_{max} of over 40%, while still maintaining an EQE above 30% at high luminance (1000 cd m^{-2}) for sensitizer-free blue OLEDs with a CIEy value smaller than 0.15 (Fig. 4f and Supplementary Table 4). The angle-dependent EL intensities of the devices based on BOCzSi and 2BOCzSi were also measured (Supplementary Fig. 19), and the resultant emission profiles exhibited near-Lambertian characteristics. Moreover, we evaluated the operational stability of devices based on BOCzSi and 2BOCzSi hosts. The BOCzSi-based device exhibited a half-lifetime (LT_{50}) of 27.4 h at an initial luminance of 562 cd m^{-2}. Comparison of the estimated LT_{50} values at 100 cd m^{-2} revealed that the BOCzSi-based device possessed a significantly longer lifetime than its 2BOCzSi-based counterpart (LT_{50}@100 cd m^{-2} = 562.1 h for BOCzSi and 118.8 h for 2BOCzSi). This enhancement is likely attributable to more efficient energy transfer and improved exciton utilization in BOCzSi. Furthermore, the LT_{50} of the BOCzSi-based device significantly exceeded those of previously reported DOBNA-derived hosts for non-sensitized OLEDs (Supplementary Fig. 20 and Supplementary Table 5). These results demonstrate the potential of BOCzSi-type materials as the host for stable blue OLEDs. To check the universality of BOCzSi and 2BOCzSi as the host materials, another blue MR-TADF material, BN-ICz-Ph, was utilized to fabricate OLED devices. The commonly used mCP host material was also selected as a comparison. As shown in Supplementary Figs. 21–23 and Supplementary Table 6, the devices with the BOCzSi as a host material exhibit the improvements in the EL performance, clearly demonstrating the advantage of this class of host materials for narrowband blue OLEDs.

To highlight the advantage of the binary non-sensitized OLED devices based on BOCzSi and 2BOCzSi, ternary HF OLEDs were fabricated for comparison using the conventional host material 2,8-bis(diphenylphosphoryl)dibenzo[b,d]furan (PPF) (Supplementary Figs. 24, 25). The device architecture was configured as follows: ITO/MoO_3 (10 nm)/TAPC (30 nm)/TCTA (10 nm)/mCP (10 nm)/PPF: 20% BOCzSi or 2BOCzSi: 1% *ν*-DABNA (20 nm)/PPF (5 nm)/TmPyPB (40 nm)/LiF (1 nm)/Al (100 nm). The identical narrowband blue emission from *ν*-DABNA can be observed in both ternary HF OLEDs and the binary systems. This phenomenon is attributed to the efficient energy transfer between the sensitizers (BOCzSi/2BOCzSi) and *ν*-DABNA. From Supplementary Table 7, it is noted that the HF devices incorporating BOCzSi and 2BOCzSi as sensitizers exhibited substantial performance enhancements compared to the PPF-based binary system (Supplementary Fig. 26). However, their performance did not exceed that of the binary system based on the BOCzSi host. This observation underscores that the rational design of non-sensitized binary systems is paramount for achieving devices with simple yet efficient architectures.

In order to elucidate the origin of the remarkable performance characteristics observed in binary non-sensitized OLEDs, we conducted a comprehensive analysis of potential contributing factors. On the one hand, the enhanced EL performance stems from optimized triplet exciton dynamics in the emitting layer[17]. As depicted in Fig. 5, upon electron-hole recombination at the TADF host, the T_1 excitons undergo RISC to populate the S_1 state, followed by FRET to the S_1 state of the terminal MR-TADF guest. This host-mediated RISC mechanism critically governs triplet exciton recycling efficiency. The rapid k_{RISC} values of both BOCzSi (3.2×10^6 s^{-1}) and 2BOCzSi (1.1×10^6 s^{-1}) significantly accelerate triplet exciton kinetics, thereby suppressing detrimental TTA and TPA processes, ultimately enhancing device efficiency[40,41]. Notably, BOCzSi exhibits a 2.9-fold higher k_{RISC} than 2BOCzSi, consistent with its shorter delayed lifetime. The efficient triplet exciton recycling and effective singlet exciton harvesting are favorable for high efficiency and low roll-off.

On the other hand, we systematically characterized the photophysical properties of their blended films incorporating *ν*-DABNA as the blue-emitting guest dopant to explore the structural and functional disparities between BOCzSi and 2BOCzSi. As evidenced in Supplementary Fig. 27, both doped films demonstrate narrowband emission predominantly originating from the *ν*-DABNA guest. Notably, the BOCzSi-doped film exhibits a neat emission profile, whereas tiny residual host emission shoulders persist in the 2BOCzSi-doped counterpart. Additionally, PLQY of 95% and 91% were measured for BOCzSi: *ν*-DABNA and 2BOCzSi: *ν*-DABNA films, respectively (Supplementary Table 8). The sharper emission features coupled with efficient PLQY values unambiguously indicate more complete FRET between BOCzSi and the terminal emitter *ν*-DABNA. According to the TRPL measurements of the doped films (Supplementary Fig. 28), the delayed fluorescence lifetimes are determined to be 1.35 and 3.06 μs for BOCzSi- and 2BOCzSi-based films, respectively, corresponding to the enhanced k_{RISC} of 0.9×10^6 and 0.5×10^6 s^{-1} (Supplementary Table 9)[24,26]. These results support the occurrence of efficient energy transfer within the host-guest systems. Moreover, it is noteworthy that the orientation of the emitter's transition dipole moment in the emissive layer (EML) significantly influences the outcoupling efficiency, ultimately determining the device's EQE. Given the low dopant concentration in host-dopant systems, the molecular architecture of the host plays a critical role in governing molecular orientation[30]. Angle-dependent PL measurements of the doped films (Supplementary Fig. 29) reveal a 91% horizontal dipole orientation for the BOCzSi-based doped film versus 85% for the 2BOCzSi counterpart. The enhanced horizontal dipole orientation observed in BOCzSi suggests its distinct potential for achieving higher performance in OLED devices[42]. In addition, the structural differences between BOCzSi and 2BOCzSi have an impact on the corresponding charge transport properties (Supplementary Fig. 29c, d). Compared to 2BOCzSi, the retention of a single carbazole

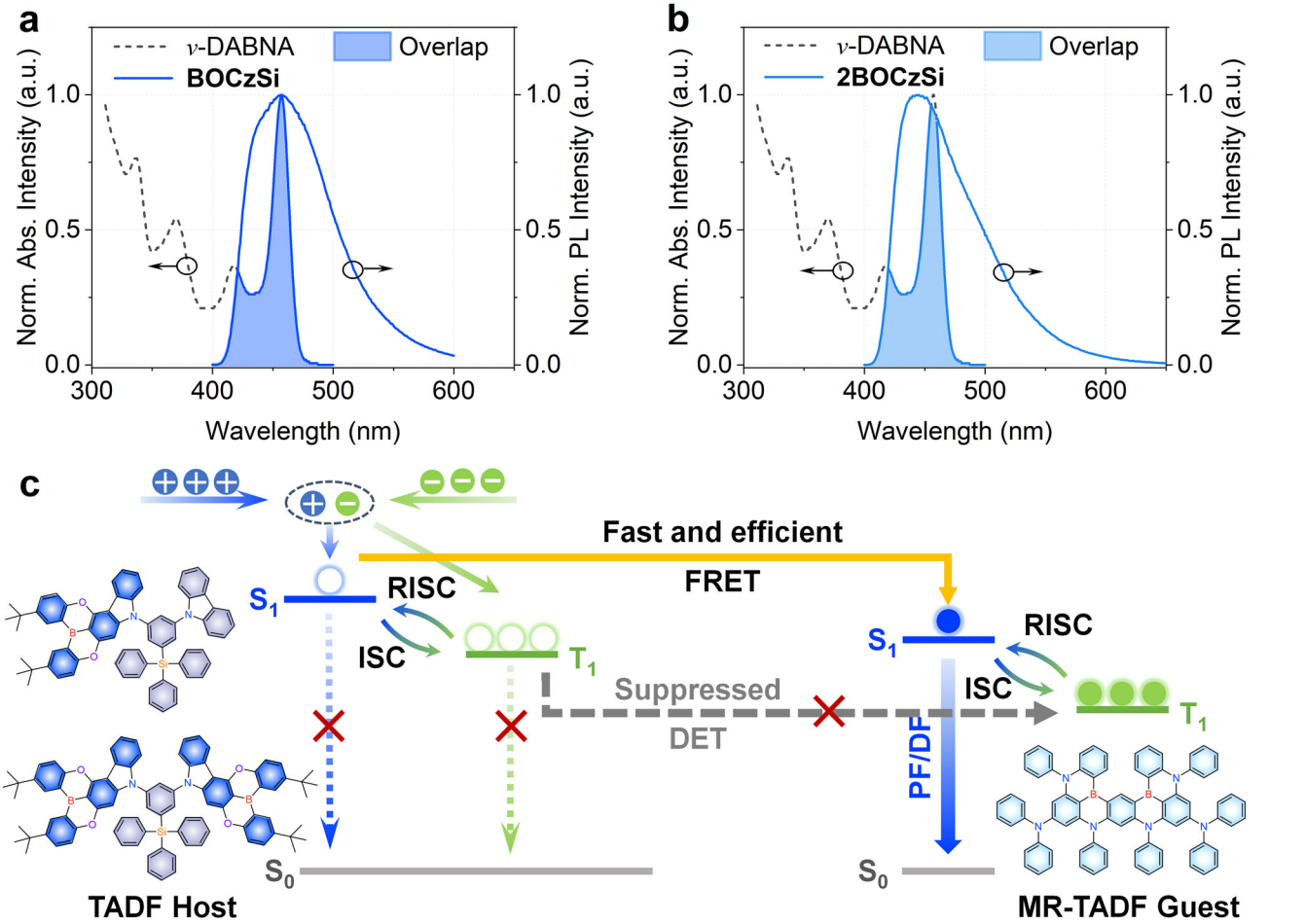

Fig. 5 | The process of energy transfer. Spectral overlap between *ν*-DABNA and **a** BOCzSi as well as **b** 2BOCzSi. **c** Schematic diagram illustrating the operational mechanism of energy transfer between the host matrix and the *ν*-DABNA dopant.

unit in BOCzSi results in more balanced charge transport characteristics, which contributes to the observed enhancement in their EL performance.

Furthermore, as illustrated in Fig. 5, the singlet exciton harvesting process by the terminal MR-TADF emitter constitutes a critical determinant of the overall photoluminescence efficiency, which is predominantly governed by host-guest FRET interactions. To evaluate the efficacy of this FRET process, we performed a direct comparative analysis of the spectral overlap among the emission spectra of BOCzSi/2BOCzSi and the absorption spectrum of the guest material *ν*-DABNA in Fig. 5. Notably, BOCzSi exhibited a more pronounced spectral overlap compared to 2BOCzSi. The maximum emission peak of BOCzSi is almost the same as the absorption peak of *ν*-DABNA, while there is a bandgap of around 4 nm between the maximum emission peak of 2BOCzSi and the absorption peak of *ν*-DABNA. Based on the spectral overlap integrals, we calculated the FRET radius and rates for BOCzSi and 2BOCzSi as 7.3 nm/$1.6 \times 10^9\ s^{-1}$ and 7.2 nm/$5.1 \times 10^8\ s^{-1}$, respectively[18,43]. Both BOCzSi and 2BOCzSi containing host-guest systems exhibit rapid FRET, and it is noteworthy that the prominent accelerated FRET rate observed in the BOCzSi-based system represents the enhanced FRET within these doped emissive layers, which is favorable for obtaining favorable EL performances.

Discussion

In this work, a functional complementarity fusion strategy is presented to develop narrowband blue OLEDs with high efficiency and suppressed efficiency roll-off. Via intramolecular cyclization engineering, a rigid BO framework was integrated with carbazole. The extended π-conjugation delocalizes the FMO distribution onto the carbazole moiety, resulting in a reduced ΔE_{ST} and an enhanced RISC process. This establishes a different molecular paradigm for BO-based host materials by incorporating the multifunctional molecular module (BOCz) to modulate the energy levels of the host materials. The highly excited triplet energy levels ($T_1 \approx 2.93$–2.95 eV) and the relatively shallow LUMO of the host can effectively prevent the potential energy back-transfer to the host, ensuring exciton confinement on the blue emitter *ν*-DABNA. These features are crucial for mitigating the exciton quenching and facilitating the efficient charge injection. Meanwhile, the TRPL measurements reveal a rapid RISC rate ($k_{RISC} = 3.2 \times 10^6\ s^{-1}$ for BOCzSi), and the emission peaks of BOCzSi and 2BOCzSi in neat films show the near-perfect spectral overlap with the absorption peak of *ν*-DABNA. Concurrently, their doped films exhibit high PLQYs exceeding 90%. Leveraging efficient FRET, a non-sensitized blue OLED based on BOCzSi has achieved an EQE_{max} exceeding 40% (41.2%) and maintains an EQE above 30% (31.6%) at high luminance (1000 cd m^{-2}), while the CIEy value remains below 0.15. These observations collectively validate the effectiveness of the multifunctional complementarity fusion strategy. This work establishes a paradigm for designing multifunctional TADF hosts via molecular hybridization, addressing critical challenges in blue OLEDs. The findings highlight the pivotal role of material design engineering and energy transfer optimization in advancing high-performance optoelectronic technologies.

Methods

Characterization of the synthesized compounds

The detailed synthesis of the hosts and general characterizations can be found in the Supplementary Information. Comprehensive characterization of the synthesized compounds included both NMR spectroscopy and high-resolution mass spectrometry. All NMR experiments (^{1}H and ^{13}C NMR) were conducted on a Bruker NEO NMR spectrometer, with chemical shifts calibrated to the internal standard tetramethylsilane (TMS). Furthermore, high-resolution mass spectral data were obtained using a Thermo Fisher Scientific Q Exactive Focus instrument.

Thermal properties

An HCT-2 thermogravimetric analyzer was employed to perform thermogravimetric analysis (TGA). The samples were heated at a rate of 10 °C/min under a continuous nitrogen flow.

Photophysical measurements

The optical properties of the synthesized compounds were investigated through ultraviolet-visible (UV-vis) absorption and photoluminescence (PL) spectroscopy. UV-vis spectra were acquired on a PerkinElmer Lambda 750 spectrophotometer, while the corresponding PL spectra were recorded using an FM-4 fluorescence spectrophotometer. The absolute photoluminescence quantum yields (PLQYs) were determined at ambient temperature under an inert atmosphere, employing a Hamamatsu Photonics C9920-02G system with an integrating sphere. Furthermore, the transient photoluminescence dynamics were characterized by measuring the PL decay curves on a Hamamatsu Photonics Quantaurus-Tau fluorescence lifetime spectrometer (model C11367-03).

Cyclic voltammetry measurements and HOMO/LUMO determination

The electrochemical characteristics of the compounds BOCzSi and 2BOCzSi were examined by cyclic voltammetry (CV). Experiments were carried out in deoxygenated *N*,*N*-dimethylformamide (DMF) containing 0.1 M tetrabutylammonium hexafluorophosphate (TBAPF6) as the supporting electrolyte. A conventional three-electrode configuration was employed, consisting of a platinum disk working electrode, a platinum wire counter electrode, and an Ag/AgCl reference electrode. The ferrocene/ferrocenium redox couple (Fc^{+}/Fc) was utilized as an internal standard for potential calibration during electrochemical characterization. The highest occupied molecular orbital (HOMO) energies of the solid film were measured via ultraviolet photoelectron spectroscopy (UPS) using unfiltered He I irradiation (21.22 eV) from a discharge lamp, with an overall energy resolution of 100 meV[26]. The lowest unoccupied molecular orbital (LUMO) energy levels were derived from the empirical relation LUMO = HOMO + Eg, where Eg represents the optical bandgap estimated from the absorption onset.

EL device fabrication and characterization

OLED devices with BOCzSi and 2BOCzSi hosts were fabricated on pre-patterned ITO-coated glass substrates (sheet resistance ≈15 Ω/sq) functioning as the bottom electrode. Prior to device fabrication, the substrates underwent sequential ultrasonic cleaning in acetone, ethanol, and deionized water (10 min per solvent cycle) followed by drying at 110 °C in an oven. Subsequent to a UV-ozone exposure period of 20 min, the ITO substrates were mounted within a high-vacuum thermal evaporation chamber (base pressure $\leq 2 \times 10^{-6}$ mbar) for the purpose of sequential deposition of organic functional layers and metallic cathodes through the utilization of a shadow mask. All organic layers were thermally evaporated at a rate of 1.0–2.0 Å/s. After the organic films were deposited, the electron injection layer (EIL) (LiF) and metal electrode (Al cathode) were deposited at rates of 0.1 and 10 Å/s, respectively. The devices were subjected to simultaneous measurement using a source meter (Keithley model 2400) and a luminance meter/spectrometer (PhotoResearch PR670).

Data availability

The data that support the findings of this study are provided in the Source Data file. Additional data are available from the corresponding authors upon request. Source data are provided with this paper.

References

1. Fan, X. et al. Ultrapure green organic light-emitting diodes based on highly distorted fused π-conjugated molecular design. *Nat. Photon.* **17**, 280–285 (2023).
2. Kim, H. S. et al. Advancing efficiency in deep-blue OLEDs: exploring a machine learning-driven multiresonance TADF molecular design. *Sci. Adv.* **11**, eadr1326 (2025).
3. Mamada, M., Hayakawa, M., Ochi, J. & Hatakeyama, T. Organoboron-based multiple-resonance emitters: synthesis, structure–property correlations, and prospects. *Chem. Soc. Rev.* **53**, 1624–1692 (2024).
4. Fan, X. et al. RGB thermally activated delayed fluorescence emitters for organic light-emitting diodes toward realizing the BT.2020 standard. *Adv. Sci.* **10**, 2303504 (2023).
5. Hua, T. et al. Deep-blue organic light-emitting diodes for ultrahigh-definition displays. *Nat. Photon.* **18**, 1161–1169 (2024).
6. Wang, Q. et al. Linear annulation engineering of indolocarbazole multiple resonance emitter to overcome efficiency-stability-color purity trilemma in deep-blue OLEDs. *Adv. Mater.* **37**, 2503839 (2025).
7. Hatakeyama, T. et al. Ultrapure blue thermally activated delayed fluorescence molecules: efficient HOMO–LUMO separation by the multiple resonance effect. *Adv. Mater.* **28**, 2777–2781 (2016).
8. Pu, Y. et al. Sulfur-locked multiple resonance emitters for high performance orange-red/deep-red OLEDs. *Nat. Commun.* **16**, 332 (2025).
9. Lee, Y. et al. Bright, efficient, and stable pure-green hyperfluorescent organic light-emitting diodes by judicious molecular design. *Nat. Commun.* **15**, 3174 (2024).
10. Wang, X. et al. Improving the stability and color purity of a BT.2020 blue multiresonance emitter by alleviating hydrogen repulsion. *Sci. Adv.* **9**, eadh1434 (2023).
11. Park, I. S., Min, H. & Yasuda, T. Ultrafast triplet–singlet exciton interconversion in narrowband blue organoboron emitters doped with heavy chalcogens. *Angew. Chem. Int. Ed.* **61**, e202205684 (2022).
12. Hu, Y. et al. Efficient selenium-integrated TADF OLEDs with reduced roll-off. *Nat. Photon.* **16**, 803–810 (2022).
13. Cheng, Y. et al. Efficient, narrow-band, and stable electroluminescence from organoboron-nitrogen-carbonyl emitter. *Nat. Commun.* **15**, 731 (2024).
14. Huang, X. et al. B–N covalent bond-involved π-extension of multiple resonance emitters enables high-performance narrowband electroluminescence. *Natl. Sci. Rev.* **11**, nwae115 (2024).
15. Chan, C. et al. Stable pure-blue hyperfluorescence organic light-emitting diodes with high-efficiency and narrow emission. *Nat. Photon.* **15**, 203–207 (2021).
16. Zeng, J. et al. Purely organic room-temperature phosphorescence sensitizers for highly efficient hyperfluorescence OLEDs. *Sci. Adv.* **11**, eadt7899 (2025).
17. Zhang, D. et al. Efficient and stable deep-blue fluorescent organic light-emitting diodes employing a sensitizer with fast triplet upconversion. *Adv. Mater.* **32**, 1908355 (2020).
18. Xiao, Z. et al. Deep-blue OLEDs with BT. 2020 blue gamut, external quantum efficiency approaching 40%. *Adv. Mater.* **37**, 2419601 (2025).

19. Stavrou, K., Franca, L. G., Danos, A. & Monkman, A. P. Key requirements for ultraefficient sensitization in hyperfluorescence organic light-emitting diodes. *Nat. Photon.* **18**, 554–561 (2024).
20. Zhang, D. et al. High-efficiency fluorescent organic light-emitting devices using sensitizing hosts with a small singlet–triplet exchange energy. *Adv. Mater.* **26**, 5050–5055 (2014).
21. Jhun, B. H. et al. The degradation mechanism of multi-resonance thermally activated delayed fluorescence materials. *Nat. Commun.* **16**, 392 (2025).
22. Hirai, H. et al. One-step borylation of 1,3-diaryloxybenzenes towards efficient materials for organic light-emitting diodes. *Angew. Chem. Int. Ed.* **54**, 13581–13585 (2015).
23. Oda, S. et al. Carbazole-based DABNA analogues as highly efficient thermally activated delayed fluorescence materials for narrowband organic light-emitting diodes. *Angew. Chem. Int. Ed.* **60**, 2882–2886 (2021).
24. Kondo, Y. et al. Narrowband deep-blue organic light-emitting diode featuring an organoboron-based emitter. *Nat. Photon.* **13**, 678–682 (2019).
25. Tanaka, H. et al. Hypsochromic shift of multiple-resonance-induced thermally activated delayed fluorescence by oxygen atom incorporation. *Angew. Chem. Int. Ed.* **60**, 17910–17914 (2021).
26. Park, D. et al. High-performance blue OLED using multiresonance thermally activated delayed fluorescence host materials containing silicon atoms. *Nat. Commun.* **14**, 5589 (2023).
27. Madayanad Suresh, S., Hall, D., Beljonne, D., Olivier, Y. & Zysman-Colman, E. Multiresonant thermally activated delayed fluorescence emitters based on heteroatom-doped nanographenes: recent advances and prospects for organic light-emitting diodes. *Adv. Funct. Mater.* **30**, 1908677 (2020).
28. Lv, X. et al. Extending the π-skeleton of multi-resonance TADF materials towards high-efficiency narrowband deep-blue emission. *Angew. Chem. Int. Ed.* **61**, e202201588 (2022).
29. Wang, F., Zhang, L., Han, W., Bin, Z. & You, J. Intramolecular C–H activation as an easy toolbox to synthesize pyridine-fused bipolar hosts for blue organic light-emitting diodes. *Angew. Chem. Int. Ed.* **61**, e202205380 (2022).
30. Madushani, B. et al. Hexacarbazolylbenzene: an excellent host molecule causing strong guest molecular orientation and the high-performance OLEDs. *Adv. Mater.* **36**, 2402275 (2024).
31. Kim, N. et al. Enhancing narrowband blue TADF OLED performance with adamantane group-integrated spatially hindered 1,3-bis(N-carbazolyl)benzene-based host. *Adv. Funct. Mater.* **34**, 2408491 (2024).
32. Li, G. et al. Asymmetric structural design of a highly oriented multi-resonance emitter enables a record 41.5% external quantum efficiency in deep-blue OLED. *Mater. Today* **73**, 30–37 (2024).
33. Wu, Y. et al. Increasing the operating lifetime of green phosphorescent organic light emitting diodes by reducing charge accumulation at the interface. *Phys. Chem. Chem. Phys.* **25**, 4598–4603 (2023).
34. Zhang, Y. et al. Multiple fusion strategy for high-performance yellow OLEDs with full width at half maximums down to 23 nm and external quantum efficiencies up to 37.4%. *Adv. Mater.* **35**, 2209396 (2023).
35. Cui, L.-S., Kim, J. U., Nomura, H., Nakanotani, H. & Adachi, C. Benzimidazobenzothiazole-based bipolar hosts to harvest nearly all of the excitons from blue delayed fluorescence and phosphorescent organic light-emitting diodes. *Angew. Chem. Int. Ed.* **55**, 6864–6868 (2016).
36. He, X. et al. An ultraviolet fluorophore with narrowed emission via coplanar molecular strategy. *Angew. Chem. Int. Ed.* **61**, e202209425 (2022).
37. Guo, L. et al. Synergetic multiple charge-transfer excited states for anti-quenching and rapid spin-flip multi-resonance thermally activated delayed fluorescence emitter. *Adv. Mater.* **37**, 2500269 (2025).
38. Wu, X., Ni, S., Wang, C.-H., Zhu, W. & Chou, P.-T. Comprehensive review on the structural diversity and versatility of multi-resonance fluorescence emitters: advance, challenges, and prospects toward OLEDs. *Chem. Rev.* **125**, 6685–6752 (2025).
39. He, X. et al. Rational medium-range charge transfer strategy toward highly efficient violet-blue organic light-emitting diodes with narrowed emission. *Adv. Mater.* **36**, 2310417 (2024).
40. Li, N. et al. Versatile host materials for both D–A-type and multi-resonance TADF emitters toward solution-processed OLEDs with nearly 30% EQE. *Adv. Mater.* **35**, 2300510 (2023).
41. Li, D. et al. Spiral donor-based host materials for highly efficient blue thermally activated delayed fluorescence OLEDs. *Chem. Eng. J.* **458**, 141416 (2023).
42. Fu, Y. et al. Boosting external quantum efficiency to 38.6% of sky-blue delayed fluorescence molecules by optimizing horizontal dipole orientation. *Sci. Adv.* **7**, eabj2504 (2021).
43. Zhang, C. et al. A π–D and π–A exciplex-forming host for high-efficiency and long-lifetime single-emissive-layer fluorescent white organic light-emitting diodes. *Adv. Mater.* **32**, 2004040 (2020).

Acknowledgements

The authors acknowledge financial support from the National Key R&D Program of China (No. 2022YFE0206100) and the National Natural Science Foundation of China (No. T2425024), the Science and Technology Development Fund (FDCT), Macao SAR (No. 0008/2022/AMJ), Bureau of Science and Technology of Suzhou Municipality (No. SYC2022144), Collaborative Innovation Center of Suzhou Nano Science & Technology, and Fundamental Research Funds for the Central Universities.

Author contributions

J.T., Y.L. and Z.Z. conceived the idea for the study and designed the experiments. G.Y. conducted the synthesis, basic property characterization, and the theoretical calculations. Y.W. performed the fabrication and characterization of the devices. J.L., Y.H. and G.C. assisted in characterizations and data analysis. G.Y. and Z.Z. wrote the manuscript. J.T. and Y.L. reviewed and edited the manuscript. All authors contributed to the manuscript and participated in the discussion of the results.

Competing interests

The authors declare no competing interests.

Additional information

Supplementary information The online version contains supplementary material available at https://doi.org/10.1038/s41467-025-65446-z.

Correspondence and requests for materials should be addressed to Zhen Zhang, Yan-Qing Li or Jian-Xin Tang.

Peer review information *Nature Communications* thanks the anonymous reviewer(s) for their contribution to the peer review of this work. A peer review file is available.